Journal of Zhejiang University SCIENCE A
ISSN 1673-565X (Print); ISSN 1862-1775 (Online)
www.zju.edu.cn/jzus; www.springerlink.com
E-mail: jzus@zju.edu.cn

3D finite element analysis of the residual stresses in butt-welded plates with modeling of the electrode-movement

F. VAKILI-TAHAMI[†1], A. H. DAEI-SORKHABI[†1], M. A. SAEIMI-S[1], A. HOMAYOUNFAR[2]

([1]*Department of Mechanical Engineering, University of Tabriz, Tabriz, Iran*)

([2]*Department of Mechanical Engineering, Islamic Azad University-Tabriz Branch, Tabriz, Iran*)

[†]E-mail: F_Vakili@Tabrizu.ac.ir; Amirsorkhabi@gmail.com

Received Dec. 17, 2007; Revision accepted May 19, 2008; Crosschecked Oct. 29, 2008

Abstract: In this paper the residual stresses in a butt-welded plate of 2.25Cr 1Mo has been analyzed using a 3D and transient finite element (FE) model. Also the effect of the welding-electrode speed has been studied using death and birth of FEs. For this purpose, a coupled thermo-mechanical FE solution has been used to obtain the temperature distribution and the resulting residual stresses. Also, the variations of the physical properties of the material with temperature have been taken into account. Results show that the residual stresses in the heat affected zone (HAZ) are maximum and change along the weld and also in the plate-thickness. It has been shown that use of the 3D and transient model will lead to more accurate and realistic results which are well compared with the experimental test data.

Key words: Finite element (FE), Residual stresses, Weldment, 2.25Cr 1Mo steel
doi:10.1631/jzus.A0720127 **Document code:** A **CLC number:** TG4

INTRODUCTION

In spite of the vast application of welding joints in the industry, still they have been considered as a weak point in the mechanical engineering design. This is due to the shortcomings of welding technology and mismatch of the mechanical properties at the joints, and, last but not least, due to the residual stresses. For the vast application of welding joints in the industry, analysis of the residual stresses in these joints is an important task in mechanical engineering design of the weldments. The effect of these stresses in fatigue and creep lifetime adds to this importance. These stresses not only cause unwanted deformation, but also reduce the fatigue and creep lifetime of the weldments. While it is known that welding can cause highly localized tensile residual stresses that often approach the yield stress of the metal, yet it is not completely understood how various parameters of the welding process influence their distributions. Such information could be helpful in making decisions about in-service inspection and the countermeasures against cracking. Because of the inherent complexities of the welding process, many factors, both process related and geometry dependent, affect the final residual stresses. There are many experimental approaches available to measure the residual stresses; however, most of them are expensive and destructive. Therefore, a general trend to study these stresses is by using numerical methods. Since the heat generated during a welding process is dissipated through convection, conduction and radiation, a severe temperature gradient would exist around the welding point. This gradient, together with the rapid quenching and the phase transformation of the melted filler will cause the residual stresses along the joint. Nevertheless, progress has been made in modeling initially one-pass and then multi-pass girth- or butt-welds. Hibbitt and Marcal (1973) modeled one-pass welds and showed that the existing temperature gradient has a major role in producing residual stresses. Masubuchi (1991) described a method for treating welds and studied the effect of major parameters on residual stresses. Murugan *et al.*(2001) modeled a multi-pass

weld and showed that the patterns of the residual stresses change in each welding pass. This has been confirmed by using the experimental measurements for welded plates with different thickness. Rybicki *et al.*(1978) and Mesler (2004) used a modified model developed by Rosenthal to produce axi-symmetric finite element (FE) model for a two-pass girth-welded pipe. The analysis represented elasto-plastic temperature dependent material behaviour and the numerical results compared well with experimental test data. Free and Goff (1989) developed an FE model to calculate the residual stresses in multi-pass welds. Dissimilar butt-welded plates were studied by Lee and Chang (2007). In all these models, some simplifying assumptions were made to deal with the inherent complexities of the welding process. These results show that the 2D modeling of the residual stresses is unable to capture the effect of the electrode movement; therefore it is needed to use a 3D model to determine the variation of the residual stress in three directions (welding direction, plate width and plate thickness).

In this paper, the butt-welding of two 2.25Cr 1Mo plates was modeled using a finite element method based software. A 3D FE model was developed and the movement of the electrode was simulated using the death and birth of elements. For this purpose a coupled thermo-mechanical solution method was used. The elasto-plastic temperature dependent material behaviour was taken into account. In this way, the along weld-joint and through thickness residual stresses were obtained.

FE MODEL

Two semi-infinite 2.25Cr 1Mo low-alloy-ferritic steel plates with width of 72 mm and thickness of 6 mm, as shown in Fig.1 were modeled. The chemical composition of the metal is given in Table 1. The weld-groove angle is 60° and due to the symmetry, only half of the weld and plates were modeled. Fig.2 shows the FE mesh of the weld and the plate. The temperature of the melted filler material is set to be 1510 °C. The plate can dissipate heat through convection, with a heat transfer coefficient of 12 W/(m^2·K) on the plate surface. The physical properties of the material given in Table 2 vary with temperature (ASM Handbook, 1993; Kou, 2003).

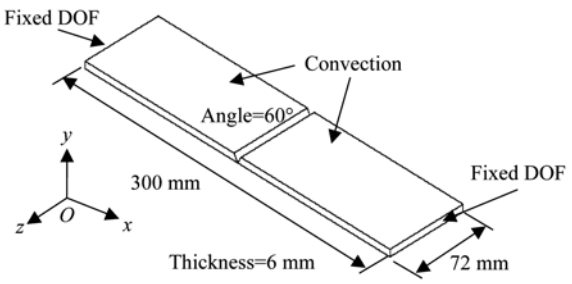

Fig.1 Joint configuration and FE boundary conditions for two semi-infinite 2.25Cr 1Mo low-alloy-ferritic steel plates with width of 72 mm and thickness of 6 mm

Table 1 Chemical composition of the metal 2.25 Cr 1Mo low-alloy-ferritic steel

Chemical composition	Mass fraction (%)	Chemical composition	Mass fraction (%)
C	0.06~0.15	S	0.03
Si	0.5	Cr	2.0~2.5
Mn	0.4~0.7	Mo	0.9~1.1
P	0.035	Cu	0.3

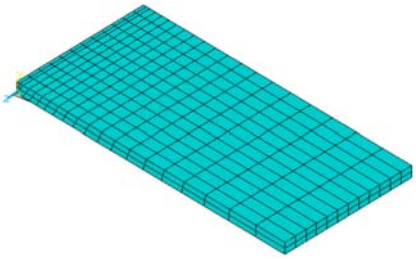

Fig.2 FE mesh of the weld and the plate

Fig.3 also shows the temperature-dependent stress-strain curve of 2.25Cr 1Mo. This curve was used to obtain yield stresses and tangent modulus at different temperature levels and to model the pre- and post-yield behaviours of the material in this study.

MODELING OF THE WELDING PROCESS

In all of the welding processes, a heat source provides the required energy and causes localized high temperature spot. In arc-welding with constant voltage V and amperage I, the efficiency of the heat source would be

$$\eta=\frac{Qt_{\text{weld}}}{VIt_{\text{weld}}}=\frac{Q}{VI}, \tag{1}$$

Table 2 Variation of the physical properties of the material with temperature (ASM Handbook, 1993; Kou, 2003)

Temp. (°C)	Density (kg/m^3)	Elastic modulus (MPa)	Poisson's ratio	Thermal expansion coefficient (K^{-1})	Thermal conductivity W/(m·K)	Specific heat (J/(kg·K))
25	7852.50	215.0	0.288	11.60	35.0	467.07
50	7850.35	212.5	0.289	12.50	36.0	473.67
100	7835.30	209.0	0.290	12.70	36.5	481.41
150	7818.65	206.0	0.292	13.30	36.5	492.53
200	7801.46	197.0	0.294	13.70	37.0	507.02
250	7782.87	194.0	0.295	14.20	36.5	524.88
300	7764.78	189.5	0.296	14.45	36.0	546.12
350	7746.16	185.0	0.297	14.70	35.5	570.74
400	7726.60	180.5	0.298	15.00	35.0	598.73
450	7706.40	177.0	0.299	15.30	34.0	630.09
500	7687.22	170.0	0.302	15.45	33.0	664.83
550	7668.35	165.0	0.305	15.55	32.0	702.95
600	7648.70	160.0	0.308	15.70	30.5	744.44
650	7630.16	155.0	0.314	15.75	28.0	784.30
700	7599.70	148.0	0.320	15.75	27.0	837.54
750	7575.98	142.0	0.330	15.75	26.0	889.16
800	7551.67	142.0	0.330	15.75	25.5	944.15
850	7526.97	142.0	0.330	15.75	25.5	1002.51
900	7501.32	142.0	0.330	15.75	25.5	1064.25
950	7475.28	142.0	0.330	15.75	25.5	1160.87
1000	7448.68	142.0	0.330	15.75	25.5	1197.88
1050	7421.54	142.0	0.330	15.75	25.5	1269.72
1100	7393.85	142.0	0.330	15.75	25.5	1344.96
1150	7365.62	142.0	0.330	15.75	25.5	1423.58
1200	7336.88	142.0	0.330	15.75	25.5	1505.57

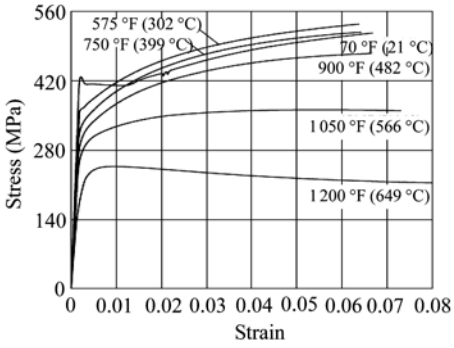

(a)

Temperature (°C)	Tangent modulus (yield elastic modulus) (MPa)
21	0
302	5.64×10^9
399	6.48×10^9
482	7.65×10^9
566	4.65×10^9
649	0

(b)

Fig.3 (a) Temperature-dependent stress-strain curve of 2.25Cr 1Mo; (b) Tangent modulus (yield elastic modulus) (ASM Handbook, 1993; Kou, 2003)

where Q is the heat generating rate, t_{weld} is the welding time and η is the thermal efficiency. During welding the governing partial differential equation for a 3D transient heat conduction, with heat generating rate Q, heat flux rate $q=-k\cdot\nabla T$ and considering density ρ, thermal conductivity k, and specific heat c as functions of temperature only, is given by the thermal equilibrium equation (Eslami and Hetnarski, 2009)

$$\rho c\frac{\partial T}{\partial t}(x,y,z,t)=-\nabla\cdot q(x,y,z,t)+Q(x,y,z,t). \quad (2)$$

Also, the equilibrium and compatibility equations are (Eslami and Hetnarski, 2009):

$$\mu\cdot u_{i,kk}+(\lambda+\mu)u_{k,ki}-(3\lambda+2\mu)\alpha T_i=0, \quad (3)$$

$$\varepsilon_{ij,kl}+\varepsilon_{kl,ij}-\varepsilon_{ik,jl}-\varepsilon_{jl,ik}=0, \quad (4)$$

where λ and μ are Lame coefficients, α is the thermal expansion and u_{ij} are displacements. These equations, together with the defined boundary conditions were

solved using an FE based coupled thermo-mechanical solution method. Fig.4 shows a schematic presentation of the butt-welding process.

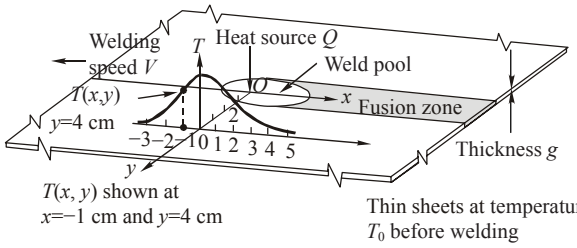

Fig.4 2D heat flow during butt-welding of two thin plates

Rosenthal proposed the following relationship to give the temperature distribution in a butt-welded plate (Kou, 2003),

$$\frac{2\pi(T-T_0)kg}{Q}=\exp\left(\frac{Vx}{2\alpha}\right)K_0\left(\frac{Vr}{2\alpha}\right), \tag{5}$$

where T is temperature, T_0 the plate temperature before welding, k thermal conductivity, g plate thickness, r radial distance from welding point, V electrode speed, and K_0 is the modified Bessel function of the second kind with zero order. Adams gave the temperature distribution as a function of the peak temperature T_p using (Deng and Murakawa, 2006)

$$\frac{1}{T_p-T_0}=\frac{4.13VYg\rho C}{Q}+\frac{1}{T_m-T_0}, \tag{6}$$

where T_m is the melting temperature, T_∞ is the ambient temperature, and Y is the vertical distance from the weld axis. Wells also used a simplified version of Rosenthal's model (Parmar, 1999),

$$Q_p=8kT_m\left(\frac{1}{5}+\frac{Vd}{4\alpha}\right),$$

where Q_p is the input heat per thickness of the plate and d is the width of molten pool. Using these relationships, the cooling-down time can be obtained. In addition to those, other models developed by Friedman (1975) or Rybicki *et al*.(1978), which are the improved or modified version of the Rosenthal's model, can be mentioned where time as an implicit parameter was used. In this paper, an improved Rosenthal's model was used in which the time of welding process was taken into account and the transient thermal analysis was carried out. Table 3 compares the simplifying assumptions made by Rosenthal (Kou, 2003) with those used in this paper.

Table 3 Comparison of the simplifying assumptions made by Rosenthal (Kou, 2003) with those used in this work

Assumption	Rosenthal's model (Kou, 2003)	Present model
Thermal analysis	2D	3D (transient)
Steady heat flow	Yes	Yes
Point heat source	Yes	Yes
Fusion heat is negligible	Yes	Yes
Physical parameters	Constant	Temperature dependent
Heat dissipation from plate surface		h=12 W/(m^2·K)
Convection in molten pool		
Thermo-mechanical analysis	Un-coupled	Coupled (transient)

The high temperature around the welding pool and the existing heat dissipation through the plate and from the surface cause a severe temperature gradient, which changes the microstructure of the metal next to the welded joint. Although the heat affected zone (HAZ) itself is composed of different layers, but in this model, it was regarded as one layer and its physical properties are given in Table 2 varying with temperature (Gery and Maropoulos, 2005).

To model the movement of the welding electrode along the z-axis (Fig.1), the weld was divided into 3 parts and the length of each part is 24 mm. With the speed of 3 mm/s for the movement of the welding electrode, each part will take 8 s to finish which is called a step. These values were adapted based on the Rosenthal's model (Kou, 2003), and it was proved that in this way, the temperature in each part can be assumed to be constant. In each step, these parts were added to the weldment (FE mesh) using birth and death technique. The heat input was applied to each part for 8 s. After one step, the elements of the second part was introduced to the FE mesh (birth of elements) and the heat source was removed from the previous part and was applied to the second part. By repeating this pattern, the third part was introduced until the welding was completed. Fig.2 shows the FE model of the weld and its boundary condition are given in Fig.1.

In the coupled thermo-mechanical analysis, there are 4 degrees of freedom among which one is the temperature. This method increases the accuracy of the model and also takes into account the mutual effects of thermal strains and temperature. Besides, a bi-linear elasto-plastic model was used to carry out the stress analysis. To obtain the bi-linear elasto-plastic model, temperature-dependent Young's modulus and Tangent modulus were used, which are given in Table 2 and Fig.3, respectively.

RESULTS AND DISCUSSION

The thermal analysis showed that after 2200 s a steady-state temperature distribution is reached in the plate. Therefore, the residual stresses at this stage were presented here. To capture the stress distribution along the plate surface including its thickness direction, two paths were defined along the x-axis that are depicted in Fig.5.

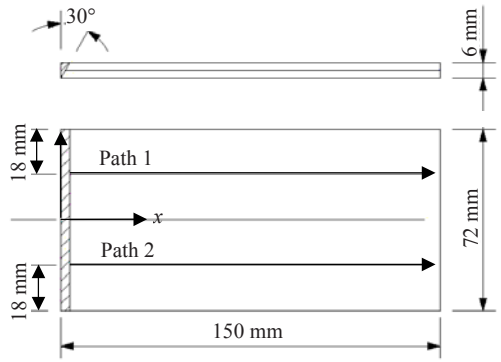

Fig.5 Two paths defined in welded plates to present the results

The results show that the plate is undergoing a significant temperature variation. Fig.6a shows the variation of the temperature distribution on the plate surface and along Path 1 at different times. It can be seen that, the maximum temperature reduces from 1015 to 350 K in 500 s. Also, this figure shows that the cooling down rate is high at the first 100 s, and then after 500 s reaches to an almost steady-state rate at 350 K. At the beginning, the temperature reduction in the area close to the weld axis shows the quenching effect; but along the path and in the area close to the plate sides the temperature increases from 298 to 350 K.

Fig.6b shows the variation of the longitudinal stress (σ_z) distribution with time for t=25, 35, 55 and 100 s on the plate surface along Path 1. Note that at t=6 s, welding electrode has passed the intersection point of Path 1 and the weld axis. This figure shows that on Path 1 and at the weld axis, stresses change from large compressive level (at t=25 s) to high tensile residual stress of 210 MPa (at t=2200 s). It also can be seen that at t=25 s, the longitudinal stresses (σ_z) on the weld material (from weld axis up to 6 mm or one times the plate thickness), increase from large compressive level of −225 to −50 MPa. However, at t=2200 s residual stresses reduce from 210 MPa at the weld axis to almost −50 MPa at x=6 mm. In other words, the maximum longitudinal residual stresses in the weld occur at a distance of one times the plate thickness. This figure also shows that for the base metal and in the region next to the weld (x=20~40 mm from the weld axis) the temperature never exceeds 600 K, and therefore the stress (σ_z) reduces from 110 MPa at t=25 s to residual stress of almost −10 MPa, and then levels out along the path to 0 MPa.

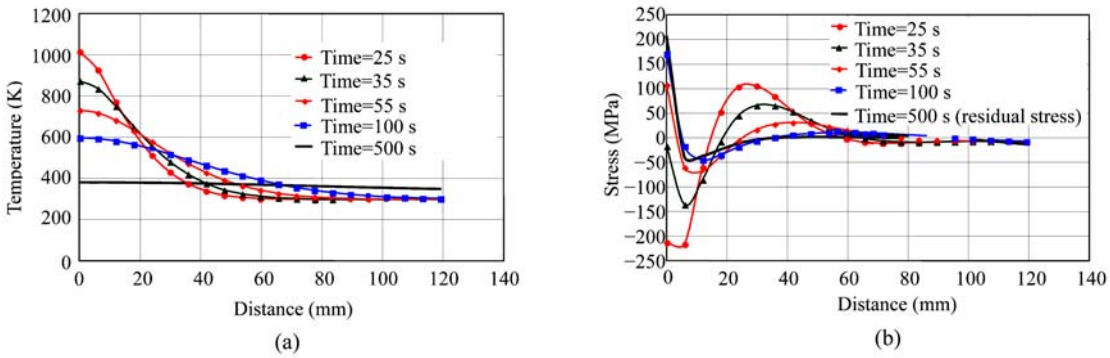

Fig.6 Distribution of (a) temperature and (b) longitudinal stress on the plate surface and along Path 1 at different times starting from 25 s up to 500 s

Fig.7a shows the variation of temperature distribution on the plate surface along Path 2, for t=40, 55, 100 and 500 s. Note that at t=18 s, welding electrode has passed the intersection point of Path 2 and weld axis.

Comparing the results shown in Fig.6a with those presented in Fig.7a shows that the heating effect caused by the welding of the previous parts leads to a higher temperature level along Path 2. The result of this effect (heating which is due to the welding itself) on the stress distribution is depicted in Fig.7b. It can be seen that the overall longitudinal residual stress (σ_z) is lower than that calculated along Path 1 (Fig.6b).

Comparing the residual stresses depicted in Figs.6 and 7 shows that at the weld-staring region (close to Path 1 shown in Fig.6), the maximum stress occurs on the weld axis; along the welding direction (towards Path 2 shown in Fig.7), the region under the tensile stress becomes wider but the stress level decreases.

Figs.8 and 9 show the variation of the temperature and longitudinal stresses with time on mid-thickness of plate, respectively. In general, the overall patterns of the temperature and stress variation repeat themselves along the surface and along the mid-thickness of the plate.

However, since a significant amount of heat dissipates from the plate surface, the temperature at the middle of the plate thickness is higher than that on the plate surface. Therefore, lower stresses were obtained in the mid of the plate comparing with those obtained on the plate surface.

CONCLUSION

This paper presented the characteristics of the residual stresses in butt-welded plates by the transient 3D coupled thermo-mechanical elasto-plastic FE analysis. The results show that:

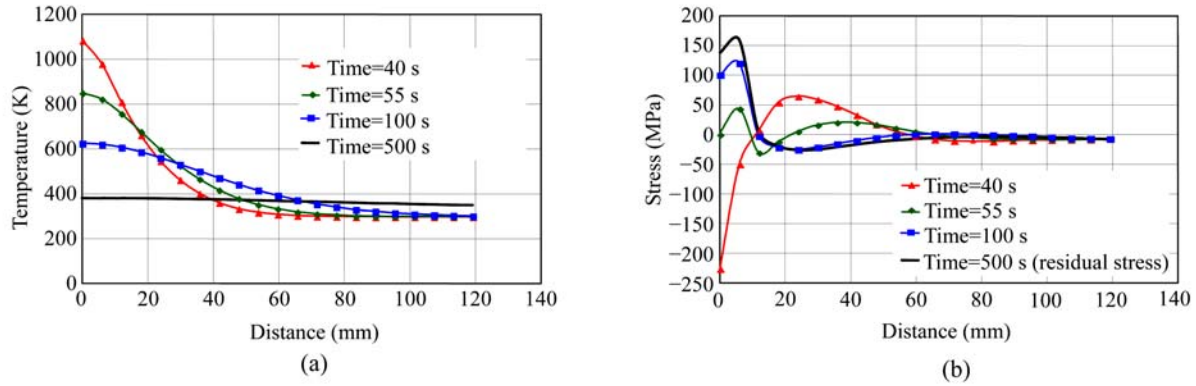

Fig.7 Distribution of (a) temperature and (b) longitudinal stress on the plate surface and along Path 2 at different times starting from 40 s up to 500 s

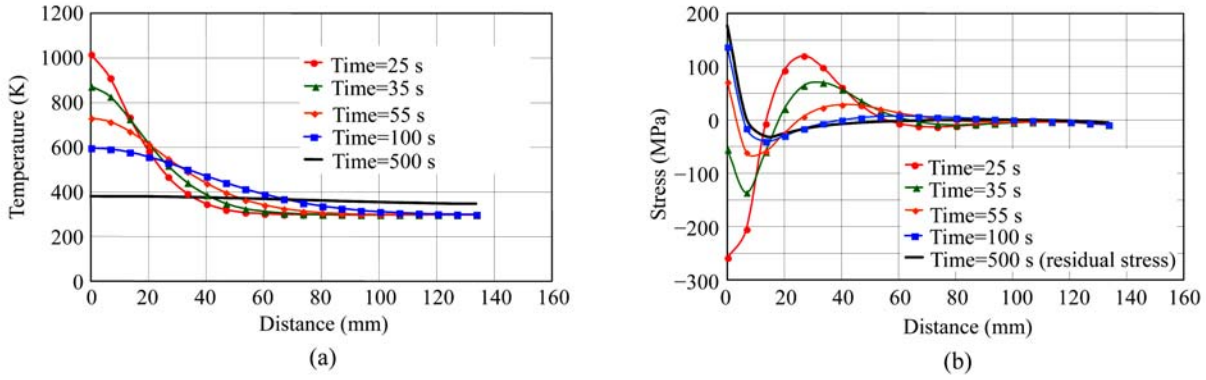

Fig.8 Distribution of (a) temperature and (b) longitudinal stress on the mid-thickness of plate and along Path 1 at different times starting from 25 s up to 500 s

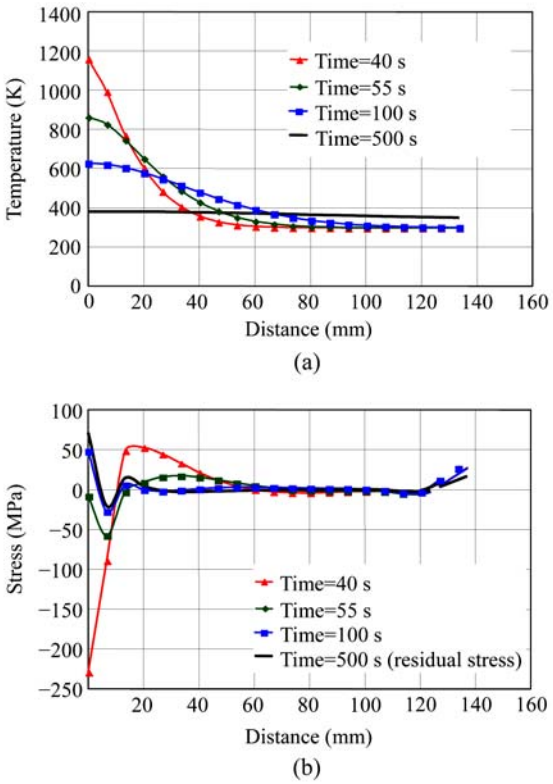

Fig.9 Distribution of (a) temperature and (b) longitudinal stress on the mid-thickness of plate and along Path 2 at different times starting from 40 s up to 500 s

(1) The maximum longitudinal residual stresses in welds occur at a distance of one times the plate thickness. In the weld-staring region, the maximum stress occurs on the weld axis; the stress decreases as moving along the welding direction, while the region under the tensile stress becomes wider.

(2) The longitudinal residual stresses change not only along the welding direction but also along the plate thickness. The stresses reduce due to the temperature gradient in the plate thickness. This shows that the plate is also under bending.

(3) The longitudinal residual stresses become insignificant at a distance of almost about 6 times of the plate thickness from the weld axis.

(4) The variation of the residual stress in three directions (welding direction, plate width and plate thickness) a 3D model should be used as that in this paper.

(5) The 3D transient FE analysis enables one to capture the variation of temperature and its gradient with time, which lead to the variation of stresses, until they reach a steady state or other residual level.

References

ASM (American Society of Metals) Handbook, 1993. Welding, Brazing and Soldering, Vol. 6, ASM International, USA.

Deng, D., Murakawa, H., 2006. Numerical simulation of temperature field and residual stress in multi-pass welds in stainless steel pipe and comparison with experimental measurements. *Computational Materials Science*, **37**(3): 269-277. [doi:10.1016/j.commatsci.2005.07.007]

Eslami, M.R., Hetnarski, R.B., 2009. Thermal Stresses—Advance Theory and Applications. Gladwell, G.M.L. (Ed.), Solid Mechanics and Its Applications, Springer, Netherlands, Vol. 158, in press.

Free, J.A., Goff, R., 1989. Predicting residual stresses in multi-pass weldments with the finite element method. *Computers and Structures*, **32**(2):365-378. [doi:10.1016/0045-7949(89)90048-5]

Friedman, E., 1975. Thermo mechanical analysis of the welding process using the finite element method. *International Journal of Pressure Vessels and Piping*, **97**:206-213.

Gery, D., Maropoulos, H., 2005. Effects of welding speed, energy input and heat source distribution on temperature variations in butt joint welding. *Journal of Materials Processing Technology*, **167**(2-3):393-401. [doi:10.1016/j.jmatprotec.2005.06.018]

Hibbitt, H.D., Marcal, P.V., 1973. A numerical thermo-mechanical model of the welding and subsequent loading of a fabricated structure. *Computers and Structures*, **3**(5):1145-1174. [doi:10.1016/0045-7949(73)90043-6]

Kou, S., 2003. Welding Metallurgy (2nd Ed.). John Wiley & Sons, Hoboken, New Jersey, p.48-52.

Lee, C.H., Chang, K.H., 2007. Numerical analysis of residual stresses in welds of similar or dissimilar steel weldments under superimposed tensile loads. *Computational Materials Science*, **40**(4):548-556. [doi:10.1016/j.commatsci.2007.02.005]

Masubuchi, K., 1991. Residual stresses and distortion in welded structures. *Welding Journal*, **70**(1212):41-47.

Messler, R.W., 2004. Principles of Welding. Wiley-Vch Verlag GmbH & Co. KGaA, Weinheim, p.162-167.

Murugan, S., Rai, S.K., Kumar, P.V., Jayakumar, T., Raj, B., Bose, M.S.C., 2001. Temperature distribution and residual stresses due to multi pass welding in type 304 stainless steel and low carbon steel weld pads. *International Journal of Pressure Vessels and Piping*, **78**(4):307-317. [doi:10.1016/S0308-0161(01)00047-3]

Parmar, R.S., 1999. Welding Engineering and Technology. Khanna Publishers, Delhi.

Rybicki, E.F., Schmueser, D.W., Stonesifer, R.W., Groom, J.J., Mishler, H.W., 1978. A finite-element model for residual stresses and deflections in girth-butt welded pipes. *International Journal of Pressure Vessels and Piping*, **100**(8):256-262.